Supporting Information

Obtaining Structural Parameters from STEM-EDX Maps of Core/Shell Nanocrystals for Optoelectronics

Jacob T. Held[1], Katharine I. Hunter[2], Nabeel Dahod[3], Benjamin Greenberg[2], Danielle Reifsnyder Hickey[1], William A. Tisdale[3], Uwe Kortshagen[2], K. Andre Mkhoyan[1*]

[1] *Department of Chemical Engineering and Materials Science, University of Minnesota, Minneapolis, Minnesota 55455, USA*

[2] *Department of Mechanical Engineering, University of Minnesota, Minneapolis, Minnesota 55455, USA*

[3] *Department of Chemical Engineering, Massachusetts Institute of Technology, Cambridge, Massachusetts 02139, USA*

*Corresponding author's contact information:

Email: mkhoyan@umn.edu

Tel: 612-625-2059

Fax: 612-626-7246

Diffusion Model

Diffusion across a core/shell interface was modelled, starting with a spherically symmetrical diffusion equation:

$$\frac{dC}{dt} = \frac{1}{r^2}\frac{d}{dr}\left[D_{AB}r^2\frac{dC}{dr}\right],$$

with:

$$C = C[r, t].$$

The following boundary and initial conditions were applied:

A. Zero- flux boundaries at the center ($r = 0$) and outer ($r = R_s$) radii of the particle:

$$\frac{dC}{dr}[0, t] = 0,$$
$$\frac{dC}{dr}[R_s, t] = 0.$$

B. The initial concentration of the core material (A) within the core ($r < R_c$) is fixed at C_{A_0} and zero in the shell ($R_c < r < R_s$):

$$C_A[0 < r < R_c, 0] = C_{A_0},$$
$$C_A[R_c < r < R_s, 0] = 0.$$

C. Similarly, for the shell material (B):

$$C_B[0 < r < R_c, 0] = 0,$$
$$C_B[R_c < r < R_s, 0] = C_{B_0}.$$

Because only species A (core material) and B (shell material) are present in the system, and they share the same crystal structure and lattice parameter:

$$C_A + C_B = 1,$$

and there is negligible interstitial population:

$$D_{AA} = D_{BB} = D_{AB} = D_{BA}.$$

The above equations were non-dimensionalized, with:

$$\theta_A = \frac{C_A}{C_{A_0}};\ \theta_B = \frac{C_B}{C_{B_0}};\ \eta = \frac{r}{R_s};\ \tau = \frac{tD_{AB}}{R_s^2};\ \chi = \frac{R_c}{R_s},$$

making the non-dimensional conservation equations for each element (A and B):

$$\frac{d\theta}{d\tau} = \frac{1}{\eta^2}\frac{d}{d\eta}\left[\eta^2\frac{d\theta}{d\eta}\right].$$

This problem was then solved with a Fourier expansion to yield $\theta_A = \theta_A[\eta, \tau, \chi]$ and $\theta_B = \theta_B[\eta, \tau, \chi]$. With incorporation of surface roughness, as described in the main text:

$$d_{surf}[\eta, \sigma] = \frac{1}{2}\left(1 - erf\left[\frac{\eta}{\sqrt{2}\sigma}\right]\right),$$

the elemental distributions using the diffusion model for the core/shell NC are analogous to eqs. [5] and [6] in the main text:

$$\theta_{Ge}[\eta, \tau, \chi, \sigma, p] = (\theta_A + p\theta_B)d_{surf}[\eta, \sigma],$$
$$\theta_{Si}[\eta, \tau, \chi, \sigma, p] = (\theta_B(1-p))d_{surf}[\eta, \sigma],$$

where p is the fraction of core material in the shell.

At low τ, this model converges to the error function model discussed in the main text. As shown in Figure S6, our particles were well within this low-τ regime, such that both models yield the same results. This means that the broadening of the Si/Ge interface can be equally discussed in terms of "roughness" or "interdiffusion". For an annealed sample in which significant diffusion occurred, such that τ is large, differences would emerge between the two models.

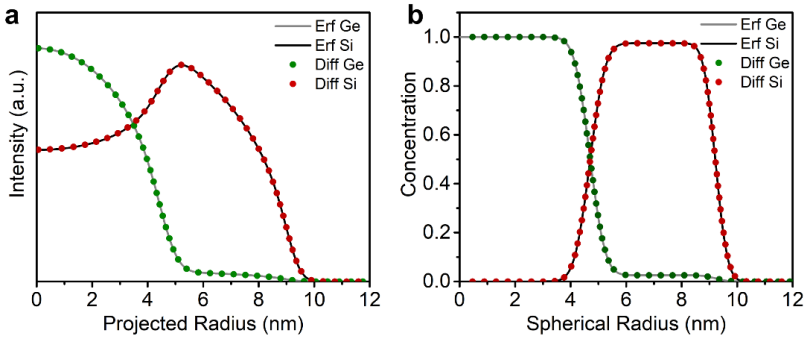

c Erf model

Parameter	Fit Value
r_{Ge}	4.69±0.07nm
r_{Si}	9.22±0.04nm
$\sigma_{Ge/Si}$	0.4 ±0.1 nm
P_{Ge}	2.5 ±0.8 %
σ_{Surf}	0.34±0.08nm

d Diffusion model

Parameter	Fit Value	
r_{Ge}	4.73	nm
r_{Si}	9.22	nm
τ	0.0011	
P_{Ge}	2.5	%
σ_{Surf}	0.37	nm

Figure S1: Comparison of the diffusion model applied to Sample 1 from Figure S6 with the error function model used in the main text. (a) Fit profiles using both models. The raw data is shown in Figure S6. (b) Radial distribution of elements from both models. (c) Fit values of each parameter in the error function model, reproduced here for convenience. (d) Fit values of each parameter in the diffusion model.

Probe Broadening Simulations

The STEM probe broadening through the sample was simulated using the Multislice method[1] with the TEMSIM package,[2] which is widely used to quantitatively model ADF-STEM images and STEM beam propagation. In this study, the STEM probe was modelled using a 60 kV beam with zero aberrations and a 25 mrad convergence angle. A 4096 x 4096 pixel^2 grid was used for the probe function over a 15 x 15 nm^2 area. The probe was then propagated through the center of a spherical 13 nm amorphous Ge nanoparticle. A cross section through the center of the probe produced the beam intensity depth profile shown in Figure S2. The intensity of the profile was then vertically summed and a Gaussian function was fit to approximate the broadening. This distribution was convoluted with a Gaussian function representing the incoherent source size (0.1 nm FWHM),[3–5] yielding a total effective probe size of 0.18 nm, which was used for the fitting procedure as described in the main text.

It should be noted that due to the small size of the nanoparticle, the overwhelming majority of the broadening arose from the convergence of the beam rather than scattering from atoms in the particle. Thus, there was little difference between the probe propagation through the nanoparticle and through vacuum, as shown in Figure S2.

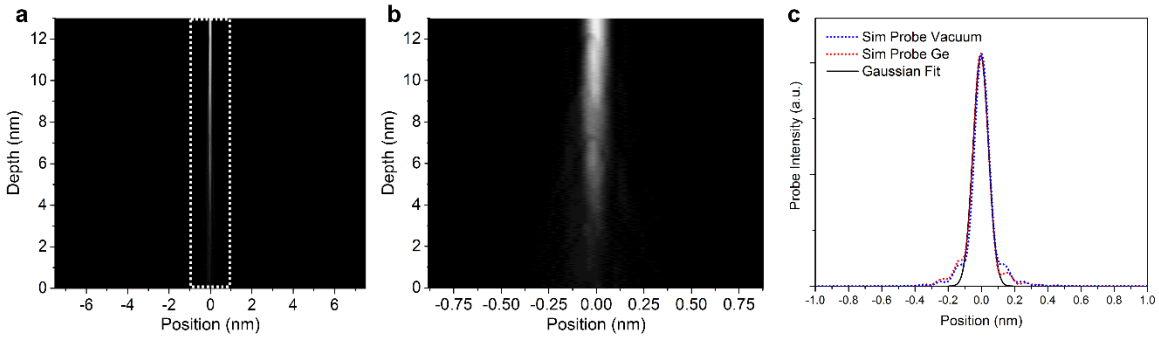

Figure S2: (a) Sample cross-section of the propagation of a simulated 60kV probe through a 13 nm diameter amorphous Ge nanoparticle. (b) Laterally expanded view of the boxed region from panel (a). (c) Intensity profiles of the probe propagated through the nanoparticle and through vacuum, shown with the Gaussian fit.

(1) Cowley, J. M.; Moodie, A. F. The Scattering of Electrons by Atoms and Crystals. I. A New Theoretical Approach. *Acta Crystallogr.* **1957**, *10* (10), 609–619.

(2) Earl J. Kirkland. *Advanced Computing in Electron Microscopy*, 2nd ed.; Springer Science & Business Media, 2010.

(3) Hillyard, S.; Silcox, J. Thickness Effects in ADF STEM Zone Axis Images. *Ultramicroscopy* **1993**, *52* (3–4), 325–334.

(4) LeBeau, J. M.; Findlay, S. D.; Allen, L. J.; Stemmer, S. Quantitative Atomic Resolution Scanning Transmission Electron Microscopy. *Phys. Rev. Lett.* **2008**, *100* (20), 206101.

(5) LeBeau, J. M.; Findlay, S. D.; Wang, X.; Jacobson, A. J.; Allen, L. J.; Stemmer, S. High-Angle Scattering of Fast Electrons from Crystals Containing Heavy Elements: Simulation and Experiment. *Phys. Rev. B* **2009**, *79* (21), 214110.

Data Analysis Flow Chart

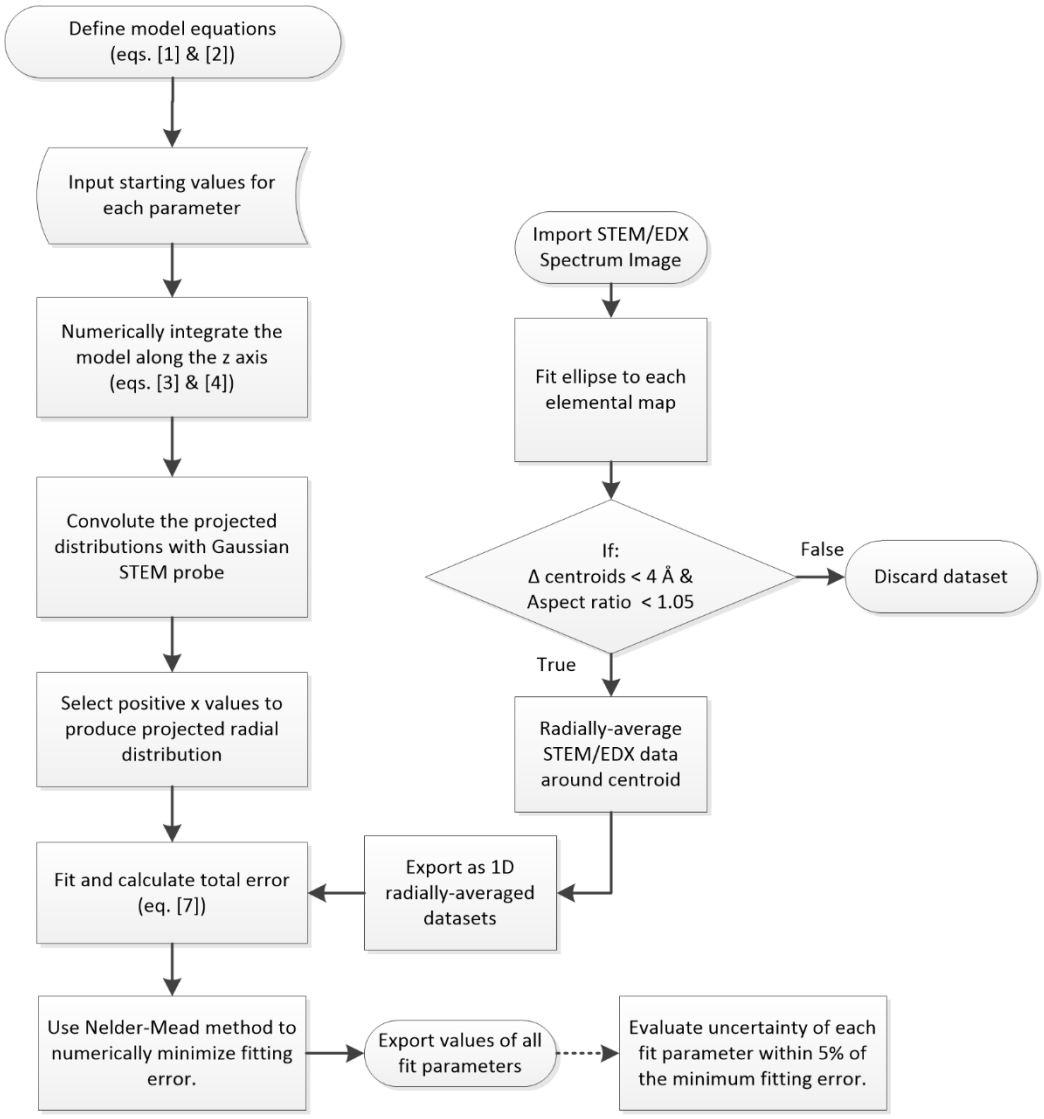

Figure S3: Flow chart of data preparation and analysis. The center fitting and radial-averaging was coded in Matlab and the radially-averaged datasets were exported to Mathematica for the main fitting procedure.

Center Determination

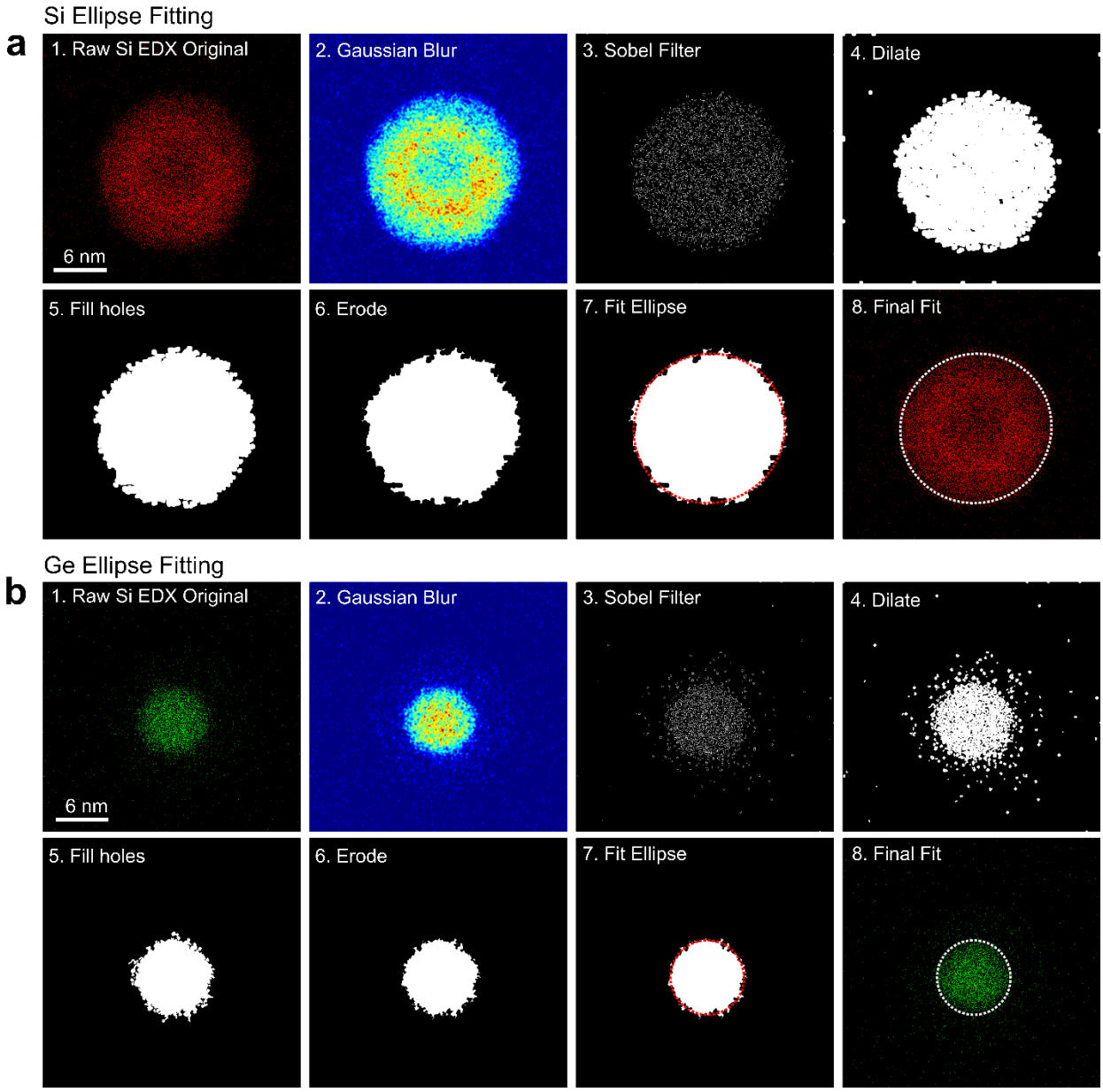

Figure S4: Ellipse fitting and center determination. **(a)** Demonstration of center determination for the Si signal from the particle analyzed in Figures 1 and 2 of the main paper, showing the intermediate steps of the procedure used: 1. Raw Si EDX signal. 2. A 3 pixel Gaussian blur was applied to smooth the raw data. 3. A Sobel filter was applied to select the significant gradients in the image. 4. The filtered image was dilated using a 5 pixel radius disk. 5. Holes were infilled. 6. The resulting image was eroded with the same 3 pixel disk used in step 3. 7. An ellipse was fit to the eroded image using the built-in regionprops function in Matlab. 8. The final image shows the fit ellipse overlaid on the raw Si EDX data. **(b)** The procedure repeated for the Ge signal from the same dataset. In this case, a 3 pixel disk was used for dilation and erosion.

Background Subtraction

A uniform Si background originating from deposition of atomic Si during NC synthesis was observed in all Ge/Si NC EDX maps. This background was removed by subtracting the average number of Si counts found outside of the NC from the dataset, as shown in Figure S5. No Ge background was observed.

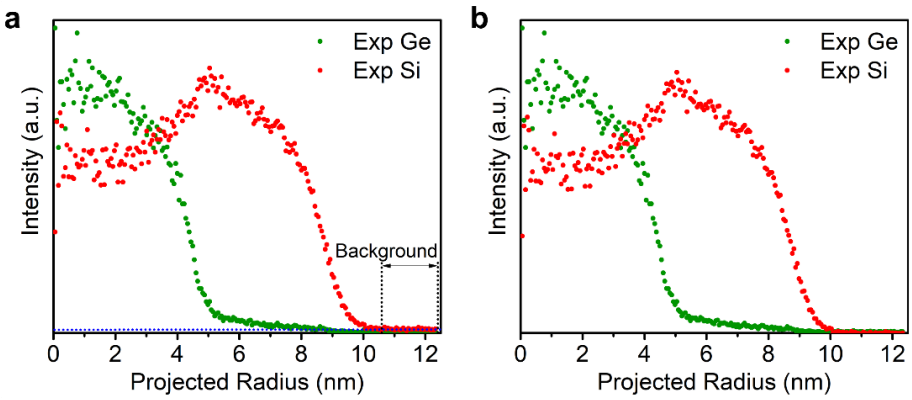

Figure S5: Background removal of the Si signal for Sample 1 shown in Figure S6. (a) The blue line shows the average value of the Si EDX signal over the highlighted background on the carbon grid away from the particle. (b) Background-subtracted raw data used for further fitting and analysis.

Supplemental Datasets

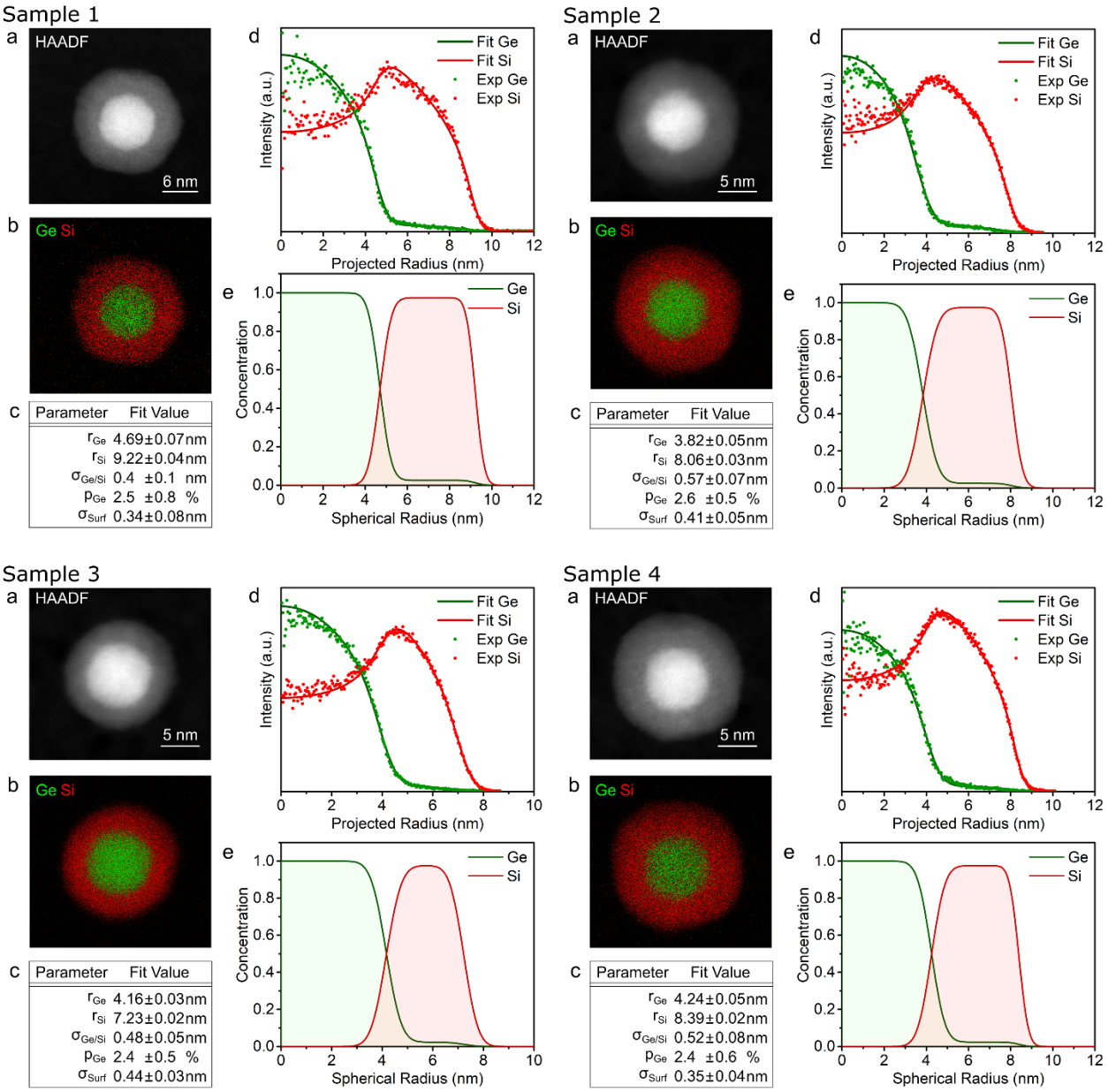

Figure S6: Analysis of four additional Si/Ge NCs using the same procedure described in the main text. The concentration of Ge in the Si shell, p_{Ge}, is similar for all NCs. For all samples: (a) HAADF-STEM image of the Ge/Si core/shell NC. (b) Composite EDX map of Ge (green) and Si (red). (c) Parameters corresponding to the optimized fit. (d) Radially-averaged EDX data with corresponding fit, with core and shell signals scaled separately. (e) Radial (spherical) distribution of Ge and Si within the NC obtained from fitting.

Electron Beam Damage

Specimen damage is the limiting factor in obtaining high-quality STEM/EDX maps from individual particles. The STEM was operated at 60 kV, mitigating knock-on damage and maximizing the cross-section for inelastic scattering, thereby increasing the efficiency of x-ray production. The particle damage was not observed to be dose-rate limited, and there was similar damage observed at low (10 pA) as well as high (150 pA) beam currents after normalizing to total electron dose. For this study, a relatively high beam current (125 pA) was used to minimize the time spent on each map acquisition.

For the Ge/Si core/shell NCs, little surface reconstruction occurred over the course of STEM/EDX map acquisition, shown in Figure S7. However, this damage was only observed around the edge of the particle, with the contrast in the center and the core/shell interface remaining unchanged. This directly shows that little to no diffusion occurred at the interface during data acquisition. It should be noted that the surface of the Ge/Si NCs was lightly oxidized during transfer between the reactor and STEM. Damage to this oxide layer is likely the source of the contrast difference observed here.

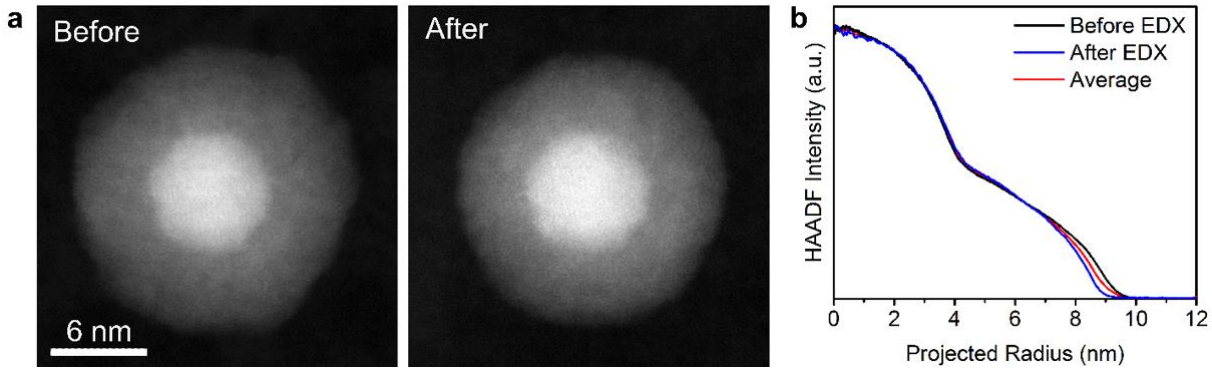

Figure S7: Ge/Si damage analysis. (a) HAADF-STEM images taken before and after STEM/EDX map acquisition for the particle shown in Figure 2 of the main text. (b) Radial profiles of the before and after images as well as the average of the two.

Damage was a larger problem in the CdSe/CdS/ZnS NCs without adequate protection. The sample was coated with 4 nm layer of alumina. During data acquisition, the alumina film itself suffered some beam damage, becoming an uneven background, precluding direct comparison of HAADF-STEM images. However, the alumina significantly reduced NC damage, and the apparent shape of the particles remained unaltered with the lattice remaining visible in HAADF-STEM. The alumina EDX features do not overlap with the features from the elements in the NCs, so this background was only present in HAADF-STEM images and had no effect on the EDX maps.

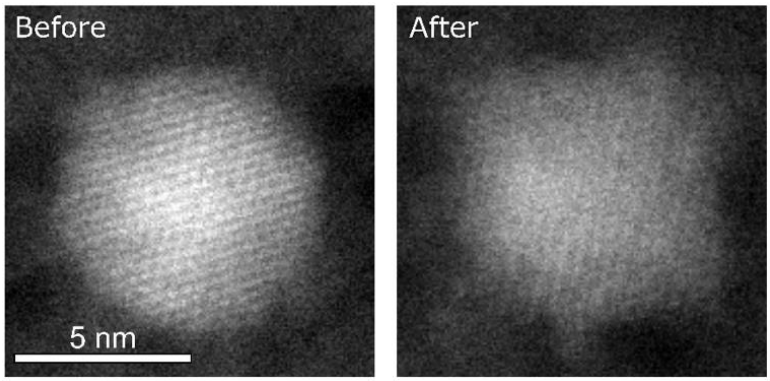

Figure S8: CdSe/CdS/ZnS damage analysis. HAADF-STEM images of the NC discussed in the main text before and after STEM/EDX acquisition. The sample was treated with 40 pulses (4 nm) of alumina ALD.

Core/Double-Shell Analysis Approach

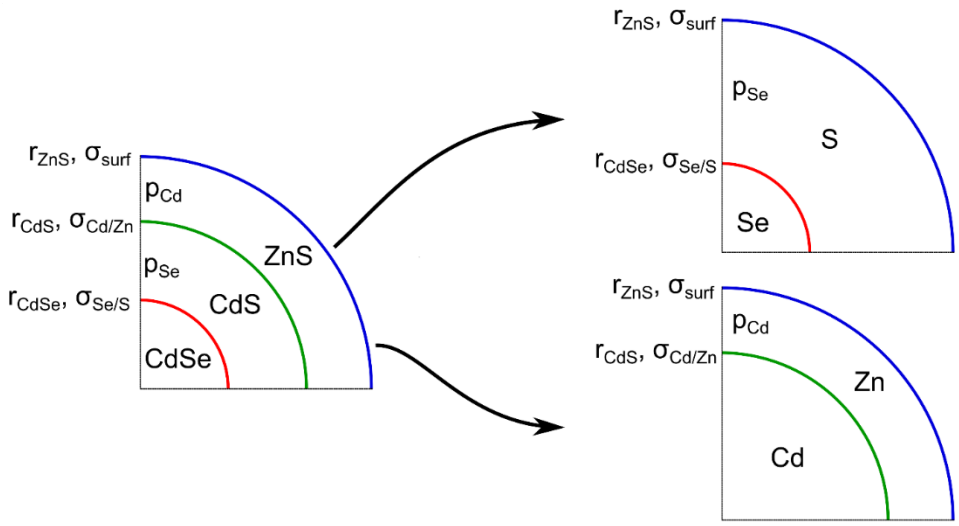

Figure S9: Schematic diagram showing the treatment of the CdSe/CdS/ZnS core double-shell NC as two core/shell NCs coupled by the surface parameters, r_{ZnS} and σ_{surf}: one representing the anions (Se and S) and the other representing the cations (Cd and Zn). Because no diffusion occurs between cations and anions, and the stoichiometry remains the same (1:1) for each layer, these two single-shell distributions are only coupled by the surface parameters.